A Marcus-Type Inverted Region in the Translocation Kinetics of a Knotted Protein

Prabhat Tripathi¹*, Behzad Mehrafrooz², Aleksei Aksimentiev², Sophie E. Jackson³, Martin Gruebele⁴*, and Meni Wanunu⁵*

KEYWORDS. Nanopore biophysics, Knotted protein, Electric field unfolding, Inverted region, Protein translocation

ABSTRACT: Knotted proteins are rare but important species, yet how their complex topologies affect their physical properties is not fully understood. Here we combine single molecule nanopore experiments and all-atom MD simulations to study the electric field-driven unfolding during the translocation through a model pore of individual protein knots important for methylating transfer RNA. One of these knots shows an unusual behavior that resembles the behavior of electrons hopping between two potential surfaces: as the electric potential driving the translocation reaction is increased, the rate eventually plateaus or slows back down in the 'Marcus inverted regime'. Our results shed light on the influence of topology in knotted proteins on their forced translocation through a pore connecting two electrostatic potential wells.

The native states of some proteins (~1% of PDB entries) contain a topological knot¹⁻⁵; for example, Haemophilus influenzae YibK and Escherichia coli YbeA 7 that act as methyl transferases, both contain a trefoil knot. Such proteins have inspired scientists to understand the mechanism by which a linear polypeptide chain spontaneously folds to form a knot8-10. Experimental studies on YibK and YbeA or other trefoil knotted methyltransferases in bulk solution have indicated the existence of several metastable intermediates and two distinct denatured configurations^{7, 11-21}. An early paper in the field suggested that, for the 52 knotted protein, one of the knot's functions could be to protect it from enzymatic degradation²². Since degradation involves the mechanical unfolding of a protein and the subsequent threading of the polypeptide chain through a narrow pore²³, it has been suggested that a knot can block the translocation of a knotted protein and even jam the degradation machinery such that it cannot degrade other proteins²⁴⁻²⁵. In addition, some computer simulations have shown that translocation of knotted protein chains requires applying a large mechanical force (>50 pN) on the terminal end ²⁴⁻²⁵, and other simulations on a long homopolymer chain have shown that knots, per se, do not prevent translocation (through a small pore $d_{pore} = 1.76$ nm), but that they introduce friction, which increases with increasing applied force.²⁶. In addition, a recent computational study has investigated the effects of topology, primary sequence, native and non-native interactions, and chain length on unfolding and translocation of a simplified model of the cellular degradation machinery, using repetitive on-off applied force²⁷. This study demonstrated that the knotted protein frequently unfolds and

translocates, but can sometimes hinder and even stall translocation under high applied force (\sim 600 pN) 28 .

In contrast, experimental studies on the degradation of knotted proteins have shown that some knotted proteins, particularly those which do not have high thermodynamic stability (as measured by reversible unfolding in chemical denaturants), can be degraded relatively easily by the bacterial degradation machine ClpXP²⁸⁻²⁹. However, in one case, a shallow trefoil-knotted protein MJ0366 fused to the larger more stable protein GFP, was unable to completely degrade²⁸. Here, it was not clear what the mechanism was - whether the knot prevented unfolding of GFP, or whether the knot was difficult to translocate. Nevertheless, in another case, it was shown that a knotted protein chain could penetrate and move through the translocation pore of ClpXP ²⁹. All of these experimental studies took an indirect approach to studying translocation by coupling it to hydrolysis of the polypeptide chain. More importantly, they only investigated a single pore size. As such, there remains much that is not known about how knotted proteins translocate through narrow pores, due to a lack of quantitative experimental studies of translocation kinetics and thermodynamics as a function of pore

In our previous single molecule-nanopore experiments, we demonstrated that electrical potential-induced unfolding drives the translocation of α -helical unknotted proteins through pores of a diameter smaller than protein size, $^{30\text{-}31}$ and that transition-state passage from unfolded to folded state and vice-versa at the surface of the pore can be resolved 32 . In this paper, we show experimentally that an electric field can drive the unfolding of the YibK and YbeA proteins, which have a complex knotted α -

¹Department of Chemistry, Indian Institute of Technology (Banaras Hindu University), Varanasi, UP-221005, India.

²Department of Physics, University of Illinois at Urbana-Champaign, Urbana, IL-61801, USA.

³Yusuf Hamied Department of Chemistry, University of Cambridge, Lensfield `Road, Cambridge CB2 1EW, UK.

⁴Department of Chemistry, University of Illinois at Urbana-Champaign, Urbana, IL-61801, USA.

⁵Department of Physics, Northeastern University, Boston, MA-02115, USA.

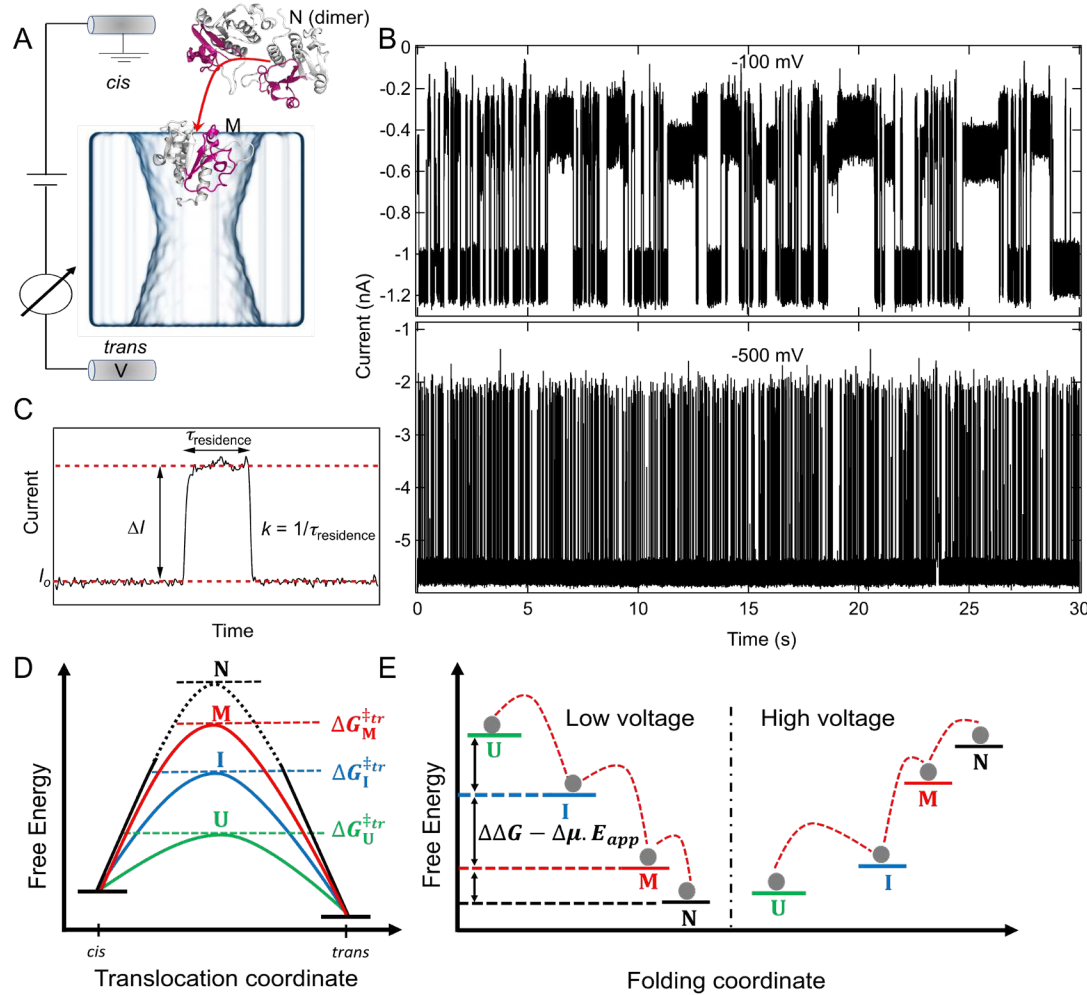


Figure 1. (A) Schematic of the nanopore experiment. Application of negative trans-pore voltage drives the single protein molecules to the pore. The interaction of a single protein molecule with a nanopore causes the blockade of ionic current. (B) Representative ionic-current recording at -100 mV and -500 mV for 0.7 μM YibK protein with a 4 nm diameter pore in 1 M KCl, 10 mM HEPES, pH 7.5. (C) Description of parameters in single-molecule current blockade events. The current blockade ratio $\Delta I/I_0$ and its duration $\tau_{\rm residence}$ provide information about the state of the protein molecules (unfolded, intermediate or fully folded) and the rate of translocation (k). (D) Energy diagram for the translocation for $d_{\rm pore} < d_{\rm protein}$. In the dimeric native state (N) the barrier for the translocation is too high to be detected, whereas the energy barrier of the monomer M or an intermediate state I lies between that for N and the unfolded state U. (E) The conformational populations of proteins are governed by thermal excitation and inherent zero-field energy gaps (ΔΔG) which are reduced and reversed by application of external electric field due to differences in the dipole moment of the conformational states.

helix/ β -sheet fold, through a pore. Our results suggest that both YibK and YbeA unfold through multiple intermediate states, and interestingly, for YbeA we observe translocation behavior that resembles the Marcus-like inverted kinetics seen in electron transport systems ³³. Our goals here are (i) to understand the transport of knotted proteins through a nanopore, and (ii) to use nanopores for observing novel molecular signatures of knotted proteins.

YibK and YbeA have almost identical molecular mass and form similar trefoil-knotted structures, but differ significantly in their stability, electric dipole moment, and charge (Table 1). YibK has a smaller electric dipole moment than YbeA, so we expect that YibK's stability and orientation is harder to perturb in the presence of the electric field. YibK is also more stable than YbeA ^{7, 11-14, 34}, therefore we expect that the translocation

of YibK for $d_{pore} < d_{protein}$, which requires at least partial unfolding, will be more difficult compared to YbeA $^{30-31}$. On the other hand, in the case of $d_{pore} > d_{protein}$ the translocation is governed by the drift-diffusion mechanism 35 , where the higher net charge on YibK protein will lead to higher drift contributions, and hence faster translocation times than YbeA.

Figure 1A shows a schematic of our experiment (details of the experimental system can be found in SI Methods and refs. $^{36-37}$). We form a nanoscale pore in a freestanding SiN membrane that bisects a fluidic cell into 'cis and trans' compartments, each containing an electrolyte solution of 1 M KCl in 10 mM HEPES buffer at pH 7.5. Applying an electric potential gradient across the compartments induces an electric field across the pore $(E_{app} = V/L_{pore})^{38}$. The applied potential V produces an ionic current through the open pore (I_o) . When a protein molecule blocks the pore, the magnitude of ionic current

reduces by an amount ΔI for some duration ($\tau_{residence}$). Typical ionic current traces for YibK measured with a 4 nm pore at -100 mV and -500 mV are shown in Figure 1B.

Table 1. Key properties of knotted protein studied here.

Protein and Source	Knot type and Location	Size (Residues, dues,	Net char ge (pH 7)	Dipole mo- ment ³⁹	Bulk unfold- ing free en- ergy ^{7,} 11-14, 34
YibK (H. in- fluen- zae)	Trefoil, residues 77-119	160, 3.95 nm	+4	241 Debye	40-50 k _B T
YbeA (E. coli)	Trefoil, residues 71-119	155, 4 nm	+2	749 Debye	20-30 k _B T

The ratio $\Delta I/I_o$ of the magnitude of change in current (ΔI) to the open pore current (I_o) (Figure 1C) gives information about the conformational state of a protein molecule (i.e., folded, intermediate, or unfolded), and the duration of blockade ($\tau_{\rm residence} = 1/k$) provides information about the rate constant k of translocation of a given state $^{30-31}$. Folded states block more current than intermediates or unfolded states, which have higher ion permeabilities. Folded states also have longer residence times because their translocation barrier is astronomically large when $d_{\rm pore} < d_{\rm protein}$, whereas intermediates or unfolded states can

translocate more rapidly. Higher E_{app} acts in analogy to a denaturant that thermodynamically stabilizes the intermediate and unfolded states $^{30\text{-}31}$ and reduces the $\Delta\Delta G$ to the native state in Figure 1E. This occurs because higher energy states (intermediate or unfolded) have larger electric dipole moments μ , so the energy $-\Delta\mu \cdot E_{app}$ has a larger magnitude. Decreasing the pore diameter (d_{pore}) increases the free energy barrier for the translocation of a given state. Thus, measurements of the distribution of $\Delta I/I_0$ and $\tau_{\text{residence}}$ as a function of E_{app} for different pore diameter allows us to identify different intermediates and unfolded states, $\Delta\Delta G$ between states and their free energy barriers for the translocation.

For experiments with the smallest pores (2 to 3 nm), only the translocation rate for YbeA increases at high voltage, whereas the more stable YibK cannot access a low-energy intermediate able to translocate through the pore (SI: Fig. S1 and Fig. S2). At the opposite extreme, for the experiments with the largest 7 nm pore, we found that >95 % of the YbeA and YibK population blocks the current very little, i.e., $\Delta I/I_0 < 0.4$ (SI: Figs. S3-S6). We attribute this to the previously demonstrated⁴⁰ weakly bound homodimeric state N either already dissociating in 1 M KCl, or dissociating to the monomeric state M when interacting with the pore, after which M is free to move through the 7 nm pore. There are known key electrostatic interactions in the interface of both of the dimers, which would be disrupted at the 1 M ionic strength to produce fast ion conductivity in our experiments ⁴⁰

In experiments with intermediate pore sizes of 4 to 5 nm (Fig. 2, SI: Fig. S7), we observed shifts in the $\Delta I/I_o$ and $\ln k$ distributions. These changes are caused by electric field-induced transitions of proteins near the pore from folded to partially un-

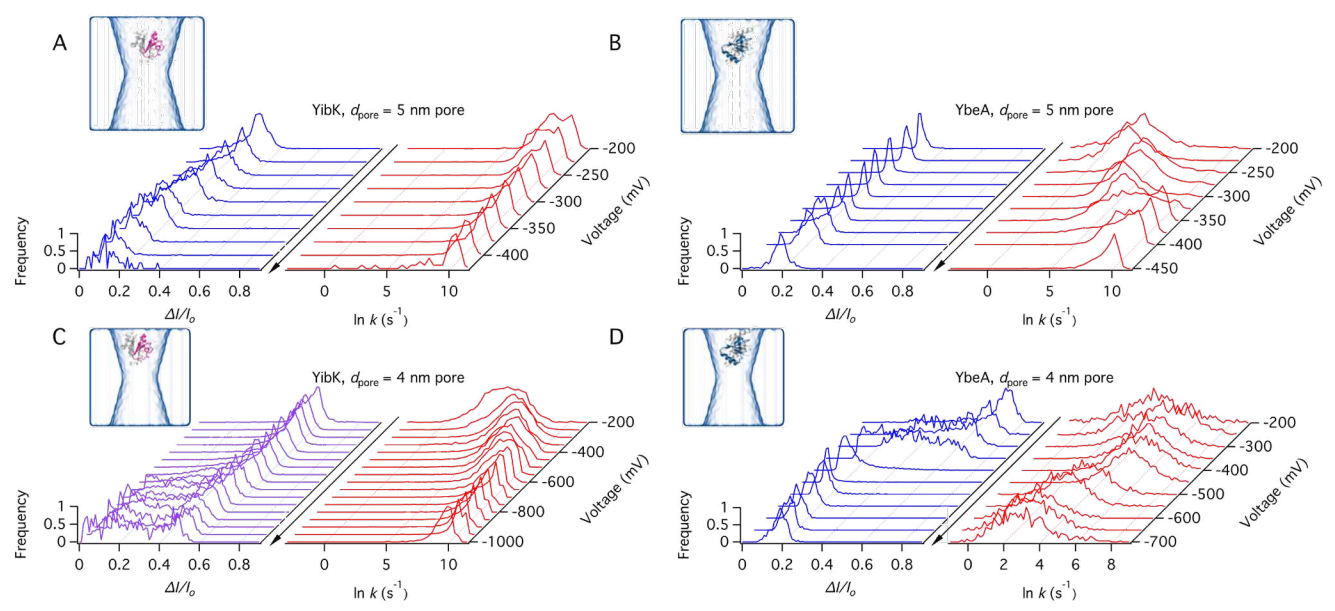


Figure 2. Electrical unfolding profile of YibK and YbeA. Distributions of $\Delta I/I_o$ and $\ln k$ as a function of voltage measured with different pore diameters for YibK and YbeA; arrows point in the unfolding direction. (A-D) For $d_{pore} = 4$ nm and $d_{pore} = 5$ nm, between -200 mV to -450 mV distributions show that for both proteins (YibK and YbeA) by increasing the magnitude of voltage, $\Delta I/I_o$ decreases and $\ln k$ increases (the data for |V| < 200 mV is shown in SI: Fig. S13ii). This is due to the electric-field stabilization of intermediate and unfolded states that lead to more permeability of ions and rapid translocation. (C) Distributions also suggest that for $d_{pore} = 4$ nm and $d_{pore} = 5$ nm, YibK translocates faster than the YbeA. $\ln k$ distributions shown in D indicates an unexpected slowing down of the translocation rate of YbeA for |V| > 450 mV as a function of driving force, not observed for YibK. Slowing down of the translocation rate for YbeA (in D) for |V| > 450 mV is explained by a non-linear dependence of free energy barrier for the U state translocation on electric field (Fig. 3) analogous to the Marcus inverted region.

folded or fully unfolded conformations that have higher ion permeability and translocation rates³⁰⁻³¹. For example, in 4 nm pores, the $\Delta I/I_o$ distributions of YbeA (Fig. 2D) show a clear transition to a lower value at \approx -450 mV, suggesting almost complete stabilization of the unfolded state, whereas the YibK $\Delta I/I_o$ distributions (Fig. 2C) show that the fully unfolded state is not highly populated even at -1 V. These results are consistent with the greater thermodynamic stability of YibK in comparison to YbeA in line with prior experiments in bulk solution.^{7, 34}

We discovered an unusual new behavior for YbeA in the 4 nm pore at voltage magnitudes that exceed -200 mV (Fig. 2CD). While the $\ln k$ distribution of YibK monotonically shifts to a higher rate as the magnitude of voltage increases from -200 mV to -600 mV, as expected when the protein loosens and unfolds through various intermediates $^{30-31}$, in contrast, $\ln k$ of YbeA shows a turnover in the rate starting at about -500 mV(Fig. 2D and SI: Fig S8-S10). Remarkably, the threshold voltage for the rate turnover is almost the same as the transition voltage in the $\Delta I/I_0$ distributions (Fig. 2D). The unexpected non-monotonic shift of the $\ln k$ distribution for YbeA was also reproduced in an experiment with a slightly smaller 3.5 nm pore (See: SI: Figs. S11-S12), so the unusual rate turnover behavior of YbeA is robust over a small range of pore diameters comparable to the protein size.

We attribute the unexpected turnover of rate for YbeA (Fig. 3A) as a function of voltage to an inverted region of YbeA translocation kinetics between potential minima on the *cis* and *trans* sides, analogous to the inverted region as a function of driving force in electron transfer (Figure 3B) ³³.

A simple approach that quantitatively explains the data in Fig. 3, in direct analogy to the electron transfer rate equation, uses the Marcus rate for a transfer reaction ⁴¹ between two diabatic potential wells:

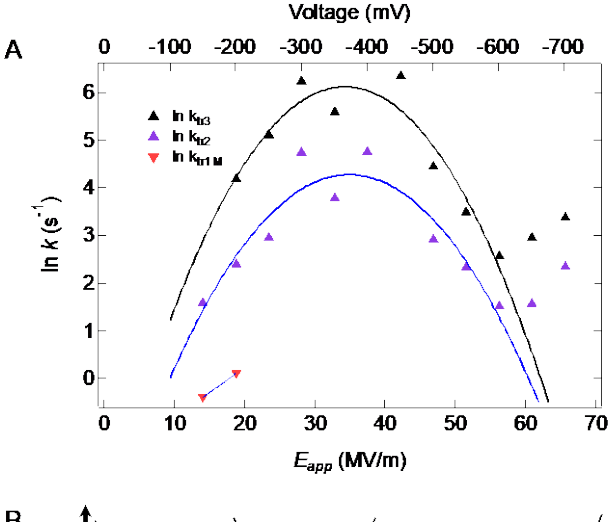
$$k = \frac{\kappa}{(4\pi\lambda k_B T)^{1/2}} exp\left[-\frac{(\lambda + \Delta G^0)^2}{4\lambda k_B T}\right],$$
 [1]

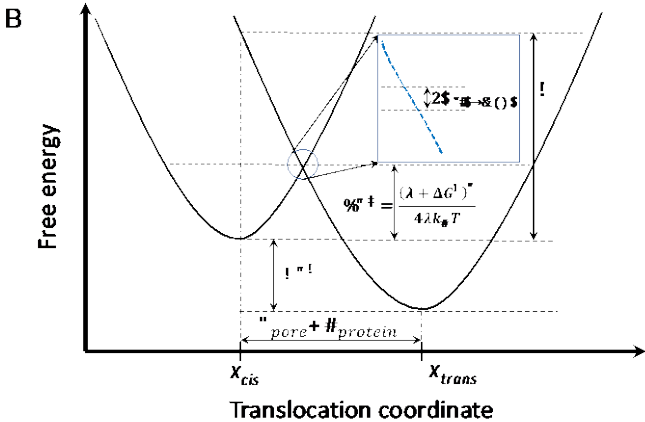
where λ , in our case, is the energy required to reorganize the protein structure from the initial (in *cis*) to final coordinates (in *trans*) before translocation, and κ is related to the coupling between the initial (*cis* side of pore) and final (*trans* side) states of the protein, (see discussion section for details about κ). ΔG^0 is the driving force for the translocation and again depends linearly on the applied electric field E_{app} as

$$\Delta G^0 = -\Delta p_{cis \to trans}. E_{ann} , \qquad [2]$$

where Δp is the difference in the dipole moment of initial and final states of the protein in the translocation reaction coordinate (i.e., $\Delta p_{cis \to trans} = p_{trans} - p_{cis}$). Using equations [1] and [2] we can fit the kinetic data in Fig. 3 (blue and black triangles) and obtained κ , $\Delta p_{cis \to trans}$ and λ for protein translocation. As shown in Table 2, we found the reorganization energy to be \approx 3.3 k_BT , which is somewhat smaller than the typical reorganization energy of rigid organic molecules ⁴², and on the order of a low protein unfolding barrier⁴³.

We note that in a recent computational study of the translocation of a knotted large homopolymer chain²⁶ (N=15,000 monomeric units, $d_{pore} = 1.76$ nm), it was reported that under large force (>30 pN) topological friction can slow down the translocation. In our case of Fig. 3A, the net force on the YbeA is < 5 pN (effective charge is +0.4e in 1 M KCl) and protein dimension ($d_{protein} = 4$ nm, N=153 residues) is comparable to the pore





size $d_{pore} = 4$ nm. Thus, our experimental condition is much dif-

Figure 3. Observation of inverted regime in the translocation rate. (A) Distributions of $ln \tau_{residence}$ for YbeA with $d_{pore} = 4$ nm were fitted (SI: Fig. S8) to identify characteristic translocation rate constants. Observed translocation rate constants (shown as symbols) are plotted as a function of E_{app}. As the electric field increases, YbeA gains access to intermediate and unfolded states and translocate through the pore. Therefore, the rate increases with E_{app} up to 35 MV/m. The rate then starts decreasing above 40 MV/m. The inversion is described by a non-linear dependence of the free energy barrier of translocation with respect to the electric field (Equation [1], black and blue solid line fits), analogous to Marcus's theory yielding a reorganization energy (Table 2) and translocation coupling constant (SI: Table S1). The slowest rate constant k_{tr1M} is assigned to translocation of the M state, the folded monomer. There may be a plateau in the rate above 55 MV/m, which could be due to alternative transition states becoming available at high energy, as has been discussed in the Marcus theory applied to proton transfer ⁶(B) Analog of Marcus kinetics in protein translocation. The reaction coordinate is now translocation from a diabatic potential well on the cis side of the pore (X_{cis}) to a potential well on the *trans* side (X_{trans}) . The barrier for transfer is determined by the intersection point of the two wells, which depends on pore length L_{pore} and diameter d_{pore} , and the reorganization energy is the energy required to transfer the protein from the cis well to the trans unfolded structure. The rate of this transfer can be described by Marcus-like kinetics, as in Equation [1]. The expanded view of the intersection of two parabolas is the adiabatic representation of the transfer with the definition of the translocation coupling constant $H_{cis \rightarrow trans}$.

ferent, and we ascribe the rate turnover mainly to activation in

the inverted region, rather than a change in the prefactor κ , which is related to friction (see discussion).

Table 2. Fitting parameters for the kinetic equation [1] in Fig.3

Data	$\kappa (k_B T s^{-1})$	$\lambda (k_B T)$	$\Delta p_{cis \to trans}$ (Debye)
Black triangle data points	2975 ± 557	3.34 ± 0.25	120 ±7
Blue triangle data points	456 ± 75	3.17 ± 0.20	112 ± 6

In addition to the phenomenological description by linear free energy relationships and Marcus theory, it would be useful to have an atomistic mechanism of how YbeA and YibK deform as they move through the pore. To gain further insight into the mechanism, we performed all-atom MD simulations to compare the two knotted proteins, YbeA and YibK. MD simulations reveal the dynamics of tightening and loosening of the knot during translocation. The simulation system contained a SiN membrane with a nanopore in it, one randomly oriented knotted monomeric protein placed above the entrance to the nanopore, and a 1 M KCl solution, Fig. 4A. Following the protocol described in our previous report ³⁰, we employed grid-steered molecular dynamics (G-SMD) ⁴⁴ to simulate the translocation of knotted proteins. Under effective electrical biases of 1.2, 0.8, or 0.5 V, complete permeation of the knotted proteins was observed for nanopores of 3.0, 3.5, and 4.0 nm diameter (Fig. 4B and SI: Fig. S13), close to the experimental size of 3.5-4.0 nm where YibK and YbeA behave differently.

As described below, the initial spatial orientation of the protein had a pronounced effect on the translocation time and the lability of the protein knot during the translocation. To evaluate changes in the protein knot geometry during the translocation, we measured the length of the knot core, which is defined

here as the number of residues between the start and the end points of the knot (Fig. 5A-B, SI Methods). Based on the RMSD of the protein backbone we found that the proteins translocate in a native-like conformation in 4 nm pores. For smaller pores and some protein orientations in the 4 nm pore, partial or complete disruption of the secondary structure was required to enable translocation (Fig. 5C). Such extensive loss of structure could lead to a high reorganization energy.

Our knot transformation analysis shows how pore diameter correlates with loosening, tightening, or maintenance of knot length (Fig. 5D). First, equilibrium simulations of the knotted proteins showed that the knot's core length fluctuates by ± 1.2 residues, as measured by the standard deviation of the knot length. We then classified as follows: upon a translocation, a knot with a length change of less than 1.2 residues is considered to have a fixed length; a knot whose length increases by more than 1.2 residues is categorized as loosening; a knot whose length decreases by more than 1.3 residues is tightening. Using this classification scheme, we computed the knots' transformation probability for our 24 nanopore translocation trajectories (Fig. 5E). A fixed-length translocation was mainly observed for the larger pore (4.0 nm), whereas in the smaller pores (3.0 and 3.5 nm), we predominantly observed either tightening or loosening of the knots, correlated with the disruption of the protein's native fold (Fig. 5F): as the RMSD of the protein backbone increases, the protein knot can either tighten or loosen, depending on the protein orientation as it enters the nanopore.

At the microscopic level, however, we found the tightening or loosening of a knot to be directly determined by the number of contacts that the knot core forms with the surrounding protein backbone: increasing the number of contacts tightens the knot whereas decreasing that number loosens it (Fig. 5G).

Our MD simulation for the 4 nm pore produces $\Delta I/I_o$ for YbeA (Fig. 4B) which is in the range of the experimental distribution of $\Delta I/I_o$ in low voltage regime ($|V|\sim200$ mV) (Fig. 2D). This was expected given that MD simulations probe the case of the non-equilibrium response of the system where the

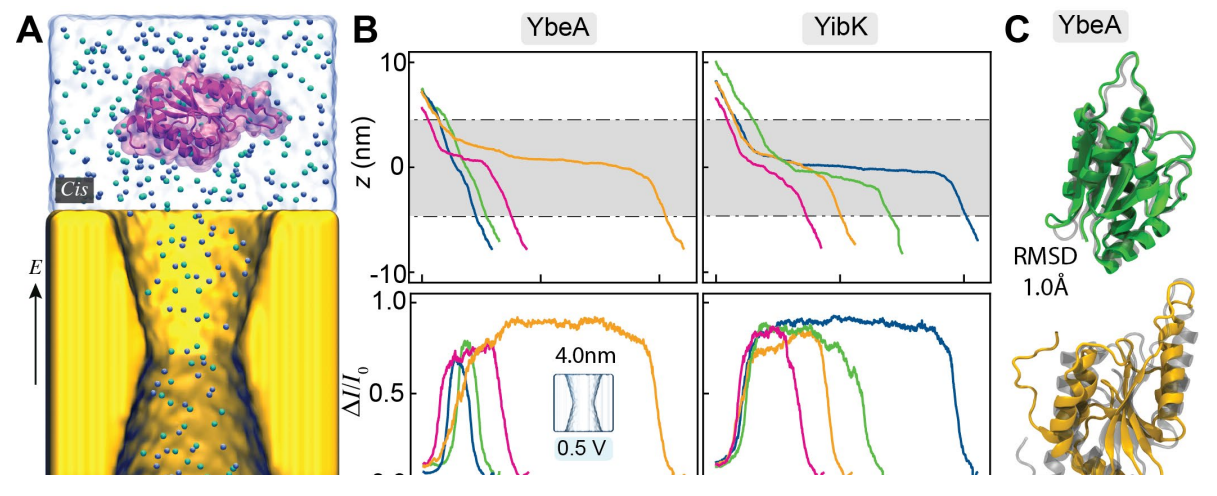


Figure 4. MD simulation of YbeA and YibK translocation. (A) Side view of the all-atom model of SiN nanopore (yellow) and a knotted protein (YbeA, shown as a cartoon enclosed by a purple semitransparent surface), submerged in a 1.0 M KCl electrolyte (transparent box with spheres as ions). (B) Protein's center of mass z-coordinate (top) and ionic current blockade (bottom) versus simulation time for G-SMD simulations carried out through a 4.0 nm nanopore. Each line shows an independent replica differing in the initial spatial orientation of the protein. The dark rectangle in top plots shows the boundaries of the pore. (C) Secondary structure of YbeA protein after the translocation through a 4.0 nm nanopore for two independent simulations. Crystal structure of the protein in shown in gray. Color of each protein matches with the traces in panel B for YbeA protein.

translocation occurs at a time scale (\sim ns) faster than the protein can equilibrate (\sim µs), whereas the experimental measurements probe the equilibrium fluctuations of protein among different states that dictate the non-equilibrium transport through the pore. Therefore, the average of $\Delta I/I_o$ for MD and that in experiments are likely to merge in the low voltage regime where protein resides mostly in the monomeric folded M state. The quantitative correlation between $\Delta I/I_o$ and $\ln k$ data (Fig. 2, SI: Fig. S1) of YbeA and YibK for different pore diameters supports the same conformation-translocation coupling mechanism that was found previously for other proteins such as cyt c and λ -repressor $^{30-32}$. The electric field governs the probability of observing different protein states via differences in their dipole moments and hence affects the translocation rate and the average current blockade ratio.

In conclusion, the most striking behavior of a knotted protein in our experiment is the inverted regime in the translocation rate behavior of YbeA for 3.5 and 4 nm pores. To interpret this result, we discuss the meaning of κ involved in the prefactor of equation [1] by considering three possible scenarios summarized in SI: Table S1. In scenario 1, κ is given by the Eyring

trans sides of the pore. More realistic is the substitution of a frictional prefactor as is done in Kramers theory, such that

$$\kappa = \frac{4\pi^2 D |H_{Cis \to trans}|^2}{L_{pore}^2 k_B T},$$
 [4]

and D/L_{pore}^{2} replaces k_BT/h . Here, D is the translational diffusion coefficient of the protein at the transition between the two potential surfaces (in the pore), estimated to be $\approx 2 \text{ nm}^2/\text{ms}$ in prior reports ³⁵, and L_{pore} is the length of the pore (10.7 nm based on the measured conductance of the pore^{36-37, 45}). This yields a *cis-trans* coupling of 0.12 k_BT , on the order of the thermal energy. A similar but somewhat smaller coupling is obtained when we replace the diffusional prefactor by a drift velocity prefactor (Vq/k_BT) D^{eff}/L_{pore}^{2} (SI: Table S1). Here the energy scale Vq of drift velocity though the pore in the potential V replaces the thermal energy scale of diffusion through the pore (q is the net charge on protein). More sophisticated Kramers-type prefactors that include different diffusion coefficients and well widths at the pore surfaces, or variable friction such as the topological friction discussed in ref. ²⁶ can yield

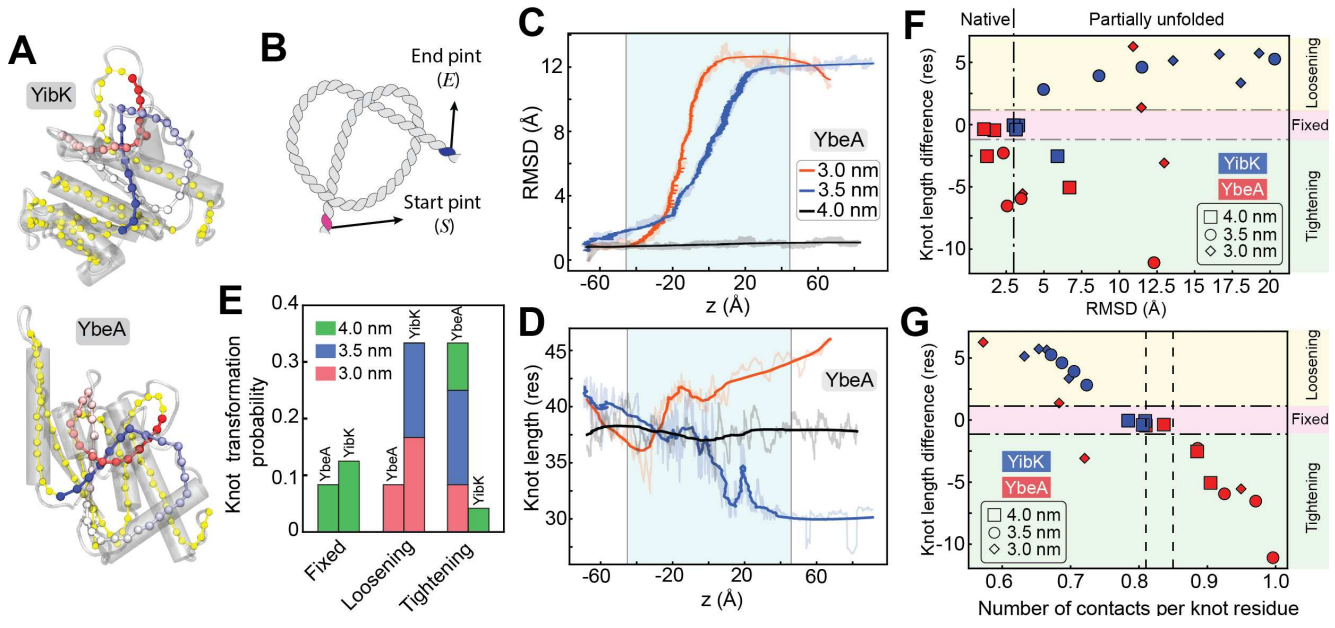


Figure 5. Protein knot lability during nanopore translocation. (A) Overall architecture of the simulated knotted proteins (YibK and YbeA) shown using a cartoon diagram (gray). To visualize the knot, the protein backbone is shown using a ball-and-stick representation, with the beginning of the knot shown in blue, the end in red, the knot's core color-mapped from blue to red. The rest of the backbone in shown in yellow. (B) Schematic representation of a 31 knot (also known as a trefoil knot) shown as a sequence of protein residues with the start and the end residues on the knot highlighted using colors. The number of residues between the start and the end points of the knot is the knot's length. (C,D) Root-mean-square deviation (RMSD) of the protein backbone coordinates (C) and the knot length (D) of a YbeA protein versus the protein's center-of-mass z-coordinate for three representative nanopore translocation trajectories. The boundaries of the nanopore membrane are shown schematically using vertical lines. Data is smoothed using a Savitzky-Golay filter with a window size of 250 and a polynomial order of two. (E) Knot's lability categorized according to the difference in the knot length before and after the nanopore transport. A knot is considered fixed if the change of the knot's length is within the range of equilibrium fluctuations (1.2 residue). The probabilities of the knot's transformation were determined based on the 24 independent MD trajectories. (F,G) Change in the knot length versus the RMSD of the protein backbone (F) or versus the normalized number of contacts between the knot core and the protein backbone (G). Native fold structures are defined as those having an RMSD of less than 3.5 Å from the crystal structure coordinates. The normalized number of contacts is defined as the number of backbone atoms within 4 Å of the knot core structure divided by the knot length. Vertical dashed lines in panel F indicate the range of the contact values seen in equilibrium simulations.

prefactor k_BT/h , or $\kappa = k_BT/h \cdot 4\pi^2 |H_{cis \to trans}|^2/k_BT$. This yields an unrealistically small value $\sim 10^{-6} k_BT$ for the coupling $H_{cis \to trans}$ between the protein potential wells on the *cis* and

larger $H_{cis \to trans} \sim k_B T$, but there is not enough data currently to justify these more sophisticated models. The key conclusion is that YbeA reaches an optimum translocation rate beyond

which additional electric field bias of the *cis* and *trans* potential wells no longer increases the rate because of the excessive structural rearrangement required, and that the coupling between the cis and trans potential wells is on the order of thermal fluctuations. The details of the translocation, as seen in simulations, are sensitive to protein orientation and interactions of the knot with other protein residues, which will have to be taken into account in a quantitative theory of the Marcus-like prefactor in eq. [1] or analogous equations (Table S1).

The data presented here clearly show that an electric field alone can facilitate the translocation of knotted protein YbeA through sub-2 nm pores without requiring a large mechanical force or an unknotting enzyme. MD simulation suggests that some of the intermediates in moderate-size pores (3-4 nm) resemble distorted native states. More detail quantitative analysis of intermediates populated during the unfolding and translocation of YbeA and YibK will be discussed in a follow-up paper. In future work, it would be intriguing to examine if the Marcuslike translocation behavior observed here for YbeA is unique to YbeA or occurs generically for proteins with low enough folding stability so that an excessive driving voltage beyond the optimum value increases the energy required for structural rearrangement and translocation.

ASSOCIATED CONTENT

Supporting Information

Detailed experimental and computational methods; example ionic current traces, extended analysis of statistics of single-molecule events such as distributions of current blockade ratio ($\Delta I/I_0$), scatter plots of $\Delta I/I_0$ and residence time ($\tau_{\rm residence}$).

AUTHOR INFORMATION

Corresponding Author

- *Prabhat Tripathi- Department of Chemistry, Indian Institute of Technology (Banaras Hindu University), Varanasi, UP 221005, India; Email: prabhat.chy@itbhu.ac.in
- *Meni Wanunu Department of Physics, Northeastern University, Boston, Massachusetts 02115, United States; Department of Chemistry & Chemical biology, Northeastern University, Boston, Massachusetts 02115, United States; Department of Bioengineering, Northeastern University, Boston, Massachusetts 02115, United States; Email: wanunu@neu.edu
- *Martin Gruebele Department of Chemistry, University of Illinois at Urbana-Champaign, Urbana, IL-61801, USA. Email: mgruebel@illinois.edu

ACKNOWLEDGMENT

We thank Amr Makhamreh for his assistance with fabrication of high-stress freestanding SiN membrane chips. We acknowledge support from the National Institutes of Health (1R21EB032640, P.T., M.W. and 1R01HG012553, B.M., A.A.), the National Science Foundation (MCB 2205665, M.G. NSF Science and Technology Center for Quantitative Cell Biology 2218365, MG, A.A.), and Science and Engineering Research Board (SRG/2023/000234, P.T.). Supercomputer time was provided through Leadership Resource Allocation MCB20012 on Frontera and through ACCESS allocation MCA05S028. Frontera is made possible by National Science Foundation award OAC-1818253.

REFERENCES

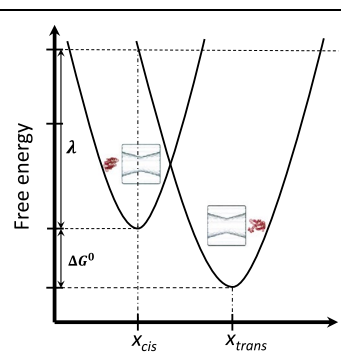
1. Mansfield, M. L., Are there knots in proteins? *Nature Structural Biology* **1994**, *I* (4), 213-214.

- 2. Taylor, W. R., A deeply knotted protein structure and how it might fold. *Nature* **2000**, *406* (6798), 916-919.
- 3. King, N. P.; Yeates, E. O.; Yeates, T. O., Identification of Rare Slipknots in Proteins and Their Implications for Stability and Folding. *Journal of Molecular Biology* **2007**, *373* (1), 153-166.
- 4. Bölinger, D.; Sułkowska, J. I.; Hsu, H.-P.; Mirny, L. A.; Kardar, M.; Onuchic, J. N.; Virnau, P., A Stevedore's Protein Knot. *PLOS Computational Biology* **2010**, *6* (4), e1000731.
- 5. Dabrowski-Tumanski, P.; Rubach, P.; Goundaroulis, D.; Dorier, J.; Sulkowski, P.; Millett, K. C.; Rawdon, E. J.; Stasiak, A.; Sulkowska, J. I., KnotProt 2.0: a database of proteins with knots and other entangled structures. *Nucleic Acids Res* **2019**, *47* (D1), D367-d375.
- 6. Silverman, D. N., Marcus rate theory applied to enzymatic proton transfer. *Biochimica et Biophysica Acta (BBA) Bioenergetics* **2000,** *1458* (1), 88-103.
- 7. Mallam, A. L.; Jackson, S. E., A Comparison of the Folding of Two Knotted Proteins: YbeA and YibK. *Journal of Molecular Biology* **2007**, *366* (2), 650-665.
- 8. Sulkowska, J. I., On folding of entangled proteins: knots, lassos, links and θ -curves. *Curr Opin Struct Biol* **2020**, *60*, 131-141.
- 9. Puri, S.; Hsu, S. D., Elucidation of folding pathways of knotted proteins. *Methods Enzymol* **2022**, *675*, 275-297.
- 10. Faísca, P. F. N., Knotted proteins: A tangled tale of Structural Biology. *Computational and Structural Biotechnology Journal* **2015**, *13*, 459-468.
- 11. Mallam, A. L.; Morris, E. R.; Jackson, S. E., Exploring knotting mechanisms in protein folding. *Proceedings of the National Academy of Sciences* **2008**, *105* (48), 18740-18745.
- 12. Mallam, A. L.; Onuoha, S. C.; Grossmann, J. G.; Jackson, S. E., Knotted Fusion Proteins Reveal Unexpected Possibilities in Protein Folding. *Molecular Cell* **2008**, *30* (5), 642-648.
- 13. Mallam, A. L.; Rogers, J. M.; Jackson, S. E., Experimental detection of knotted conformations in denatured proteins. *Proceedings of the National Academy of Sciences* **2010**, *107* (18), 8189-8194.
- 14. Mallam, A. L.; Jackson, S. E., Probing Nature's Knots: The Folding Pathway of a Knotted Homodimeric Protein. *Journal of Molecular Biology* **2006**, *359* (5), 1420-1436.
- 15. Capraro, D. T.; Jennings, P. A., Untangling the Influence of a Protein Knot on Folding. *Biophys J* **2016**, *110* (5), 1044-51.
- 16. Andrews, B. T.; Capraro, D. T.; Sulkowska, J. I.; Onuchic, J. N.; Jennings, P. A., Hysteresis as a Marker for Complex, Overlapping Landscapes in Proteins. *J Phys Chem Lett* **2013**, *4* (1), 180-188.
- 17. Burban, D. J.; Haglund, E.; Capraro, D. T.; Jennings, P. A., Heterogeneous side chain conformation highlights a network of interactions implicated in hysteresis of the knotted protein, minimal tied trefoil. *J Phys Condens Matter* **2015**, *27* (35), 354108.
- 18. Puri, S.; Liu, C. Y.; Hu, I. C.; Lai, C. H.; Hsu, S. D.; Lyu, P. C., Elucidation of the folding pathway of a circular permutant of topologically knotted YbeA by tryptophan substitutions. *Biochem Biophys Res Commun* **2023**, *672*, 81-88.
- 19. Hsu, S. D.; Lee, Y. C.; Mikula, K. M.; Backlund, S. M.; Tascón, I.; Goldman, A.; Iwaï, H., Tying up the Loose Ends: A Mathematically Knotted Protein. *Front Chem* **2021**, *9*, 663241.
- 20. Ko, K. T.; Hu, I. C.; Huang, K. F.; Lyu, P. C.; Hsu, S. D., Untying a Knotted SPOUT RNA Methyltransferase by Circular Permutation Results in a Domain-Swapped Dimer. *Structure* **2019**, *27* (8), 1224-1233.e4.
- 21. Chuang, Y. C.; Hu, I. C.; Lyu, P. C.; Hsu, S. D., Untying a Protein Knot by Circular Permutation. *J Mol Biol* **2019**, *431* (4), 857-863.
- 22. Virnau, P.; Mirny, L. A.; Kardar, M., Intricate Knots in Proteins: Function and Evolution. *PLOS Computational Biology* **2006**, *2* (9), e122.
- 23. Matouschek, A., Protein unfolding an important process in vivo? *Current Opinion in Structural Biology* **2003**, *13* (1), 98-109.
- 24. Huang, L.; Makarov, D. E., Translocation of a knotted polypeptide through a pore. *The Journal of Chemical Physics* **2008**, *129* (12), 121107.
- 25. Wojciechowski, M.; Gómez-Sicilia, À.; Carrión-Vázquez, M.; Cieplak, M., Unfolding knots by proteasome-like systems: simulations of the behaviour of folded and neurotoxic proteins. *Molecular BioSystems* **2016**, *12* (9), 2700-2712.
- 26. Rosa, A.; Di Ventra, M.; Micheletti, C., Topological jamming of spontaneously knotted polyelectrolyte chains driven through a nanopore. *Phys Rev Lett* **2012**, *109* (11), 118301.

- 27. Fonseka, H. Y. Y.; Javidi, A.; Oliveira, L. F. L.; Micheletti, C.; Stan, G., Unfolding and Translocation of Knotted Proteins by Clp Biological Nanomachines: Synergistic Contribution of Primary Sequence and Topology Revealed by Molecular Dynamics Simulations. *J Phys Chem B* **2021**, *125* (27), 7335-7350.
- 28. San Martín, Á.; Rodriguez-Aliaga, P.; Molina, J. A.; Martin, A.; Bustamante, C.; Baez, M., Knots can impair protein degradation by ATP-dependent proteases. *Proc Natl Acad Sci U S A* **2017**, *114* (37), 9864-9869.
- 29. Sivertsson, E. M.; Jackson, S. E.; Itzhaki, L. S., The AAA+ protease ClpXP can easily degrade a 31 and a 52-knotted protein. *Scientific Reports* **2019**, *9* (1), 2421.
- 30. Tripathi, P.; Benabbas, A.; Mehrafrooz, B.; Yamazaki, H.; Aksimentiev, A.; Champion, P. M.; Wanunu, M., Electrical unfolding of cytochrome c during translocation through a nanopore constriction. *Proceedings of the National Academy of Sciences* **2021**, *118* (17), e2016262118
- 31. Tripathi, P.; Firouzbakht, A.; Gruebele, M.; Wanunu, M., Threading single proteins through pores to compare their energy landscapes. *Proceedings of the National Academy of Sciences* **2022**, *119* (39), e2202779119.
- 32. Tripathi, P.; Firouzbakht, A.; Gruebele, M.; Wanunu, M., Direct Observation of Single-Protein Transition State Passage by Nanopore Ionic Current Jumps. *The Journal of Physical Chemistry Letters* **2022**, *13* (25), 5918-5924.
- 33. Miller, J. R.; Calcaterra, L. T.; Closs, G. L., Intramolecular long-distance electron transfer in radical anions. The effects of free energy and solvent on the reaction rates. *Journal of the American Chemical Society* **1984**, *106* (10), 3047-3049.
- 34. Mallam, A. L.; Jackson, S. E., Folding Studies on a Knotted Protein. *Journal of Molecular Biology* **2005**, *346* (5), 1409-1421.
- 35. Larkin, J.; Henley, R. Y.; Muthukumar, M.; Rosenstein, Jacob K.; Wanunu, M., High-Bandwidth Protein Analysis Using Solid-State Nanopores. *Biophysical Journal* **2014**, *106* (3), 696-704.
- 36. Kim, M. J.; Wanunu, M.; Bell, D. C.; Meller, A., Rapid Fabrication of Uniformly Sized Nanopores and Nanopore Arrays for Parallel DNA Analysis. *Advanced Materials* **2006**, *18* (23), 3149-3153.

- 37. Wanunu, M.; Dadosh, T.; Ray, V.; Jin, J.; McReynolds, L.; Drndić, M., Rapid electronic detection of probe-specific microRNAs using thin nanopore sensors. *Nature Nanotechnology* **2010**, *5* (11), 807-814.
- 38. Wanunu, M.; Morrison, W.; Rabin, Y.; Grosberg, A. Y.; Meller, A., Electrostatic focusing of unlabelled DNA into nanoscale pores using a salt gradient. *Nature Nanotechnology* **2010**, *5* (2), 160-165.
- 39. Felder, C. E.; Prilusky, J.; Silman, I.; Sussman, J. L., A server and database for dipole moments of proteins. *Nucleic Acids Research* **2007**, *35* (suppl_2), W512-W521.
- 40. Mallam, A. L.; Jackson, S. E., The dimerization of an alpha/beta-knotted protein is essential for structure and function. *Structure* **2007**, *15* (1), 111-22.
- 41. Zhou, H. X.; Szabo, A., Microscopic formulation of Marcus' theory of electron transfer. *The Journal of Chemical Physics* **1995**, *103* (9), 3481-3494.
- 42. Shluger, A. L.; Grutter, P., Reorganization takes energy. *Nature Nanotechnology* **2018**, *13* (5), 360-361.
- 43. Liu, F.; Nakaema, M.; Gruebele, M., The transition state transit time of WW domain folding is controlled by energy landscape roughness. *The Journal of Chemical Physics* **2009**, *131* (19), 195101.
- 44. Wells, D. B.; Abramkina, V.; Aksimentiev, A., Exploring transmembrane transport through α-hemolysin with grid-steered molecular dynamics. *The Journal of chemical physics* **2007**, *127* (12), 09B619.
- 45. Kowalczyk, S. W.; Grosberg, A. Y.; Rabin, Y.; Dekker, C., Modeling the conductance and DNA blockade of solid-state nanopores. *Nanotechnology* **2011**, *22* (31), 315101.

Table of content graphic



Translocation coordinate